Release of colloids in saturated porous media under transient hydro-chemical conditions: A pore-scale study

Safna Nishad [a], Riyadh I. Al-Raoush [a,*], Motasem Y.D. Alazaiza [b]

[a] Department of Civil and Architectural Engineering, Qatar University, P.O Box 2713, Doha, Qatar
[b] Department of Civil and Environmental Engineering, College of Engineering, A'Sharqiyah University, 400, Ibra, Oman

GRAPHICAL ABSTRACT
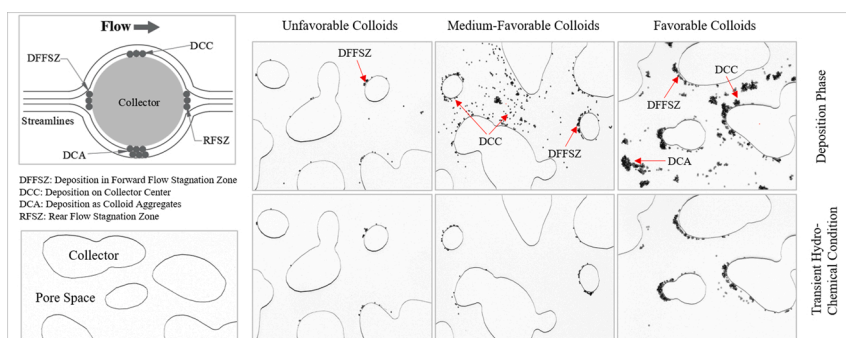
DFFSZ: Deposition in Forward Flow Stagnation Zone
DCC: Deposition on Collector Center
DCA: Deposition as Colloid Aggregates
RFSZ: Rear Flow Stagnation Zone

ARTICLE INFO

ABSTRACT

The deposition and consequent release of colloids pose a significant challenge to the environment, groundwater quality and human health. Subsurface soil contains numerous types of colloids that exhibit a diverse range of interaction favorability with the soil grains and their impact on release behavior remains unclear. The objective of this study was to investigate, at the pore-scale, the impact of colloid interaction favorability on colloid deposition and subsequent release in response to perturbations of flow rate and solution chemistry in saturated porous media. Pore-scale experiments were conducted using a micromodel that is geometrically representative of a real sand-stone rock. Favorable, medium-favorable and unfavorable colloids (i.e., repulsion absent, repulsion at long-range of separation distances and attraction absent with the micromodel surface, respectively) were deposited in the micromodel and then a series of colloid release experiments were conducted at different conditions including increasing the flow rate, decreasing the ionic strength and increasing the solution pH. Favorable colloids exhibited extensive deposition on the collector center where the flow streamlines are parallel to the collector surface, as adhesion forces overcome hydrodynamic forces. However, at medium and high ionic strength, deposition in Forward Flow Stagnation Zone (FFSZ) was dominant for unfavorable colloids as the hydrodynamic forces are negligible. Pore-scale images showed that, upon perturbations in flow rate and solution chemistry, colloids that were initially deposited on collector centers were more susceptible to release as compared to colloids that were initially deposited in FFSZs. The negligible hydrodynamic drag forces in FFSZ and deep primary minimum interaction at short separation distances were the major factors that hindered the release

of colloids in FFSZ under transient hydro-chemical conditions. The intensity of colloid deposition and release decreases as the favorability of colloids decreases and as the ionic strength decrease for unfavorable colloids. This study provides a clear insight to the pore-scale colloid deposition and release mechanisms during transient hydro-chemical conditions that help in the modeling of environmental and engineering applications including managed aquifer recharge, groundwater contamination and wastewater treatment processes.

1. Introduction

Subsurface soil contains numerous types of colloids including clay colloids, metal oxides, bacteria and viruses suspended in the pore water or deposited on soil grains [1]. Understanding the behavior of different types of colloids in natural porous media is important for environmental and engineering applications such as groundwater recharge and contamination and wastewater treatment processes [2–4]. The deposition and consequent release of colloids pose a significant challenge to the environment, groundwater quality and human health. Although colloids are immobile under natural groundwater conditions, heavy rainfall or activities of managed aquifer recharge change hydro-chemical conditions which in turn induces the release of deposited colloids [5,6]. The retention and release of colloids in porous media are affected by surface interactions where most colloids and natural soil grains tend to have a low isoelectric point resulting in negative surface charges and repulsion among them [7]. Therefore, the majority of previous studies related to colloid retention and release focused on unfavorable colloids where repulsive interaction forces are present [8–11]. However, in natural conditions, some microorganisms and metal colloids may have a positive charge that yields favorable colloid interaction with soil grains [12,13].

Although the retention behavior of favorable colloids was extensively investigated using colloid filtration theory (CFT), colloid release mechanisms have not been studied in detail [14,15]. Previous studies have focused on laboratory column experiments to quantitatively evaluate the release of unfavorable colloids based on breakthrough curves upon perturbations in flow rate or solution chemistry [16–21]. Moreover, some studies used modeling approaches to predict colloid release [22–25]. However, predictions of such modeling studies deviate from findings obtained from experiments due to the inability to incorporate mechanisms that take place at the pore-scale such as bridging, clogging, attachment on low flow zones or nanoscale surface heterogeneities. Therefore, a clear understanding of pore-scale processes through visualization studies is essential to understand the deposition and release of colloids to understand and accurately model applications such as managed aquifer recharge, groundwater contamination and wastewater treatment processes.

The release of colloids from grain surfaces depends on the relative strength of adhesive forces, torque resistance as well as hydrodynamic forces and torques applied [26–30]. Adhesive forces are greatly influenced by the solution chemistry (i.e., ionic strength, pH, and ionic composition), whereas the hydrodynamic forces increase as flow velocity increase [16,20,28,31]. Therefore, changes in the chemical composition of the aqueous phase and flow rate affect the release of colloids attached to solid surfaces. Colloids interacting with grain surfaces in the secondary minimum tend to be released upon reduction of solution ionic strength as the secondary minimum vanishes at low ionic strength conditions. However, the release of colloids in the primary minimum is negligible [32,33]. On the other hand, the release of colloids from a smooth surface is insignificant under favorable conditions and at high ionic strength for unfavorable conditions as the DLVO (Derjaguin, Landau, Verwey and Overbeek) theory predicts an infinite depth of primary minimum at these conditions [34–37]. Nevertheless, nanoscale roughness on the collector surface affects the deposition and release of colloids regardless of the theory [38–40]. For example, the presence of nanoscale physical asperities on the collector surface increase colloid deposition in secondary minima and release colloids attached in primary minima [41–43].

Colloid release during transient hydro-chemical conditions in saturated porous media has been studied using laboratory column experiments under unfavorable conditions [16–21]. Changes of colloid breakthrough in response to perturbations in flow rate and solution chemistry were observed under different colloid-collector size ratios, solution ionic strength and surface heterogeneities. The DLVO theory failed to explain some observations from such column experiments such as the fractional release of colloids when decreasing the ionic strength to which the adhesive forces are highly repulsive [36,37]. Therefore, column experiments are not quite adequate to identify deposition and release mechanisms at the pore-scale including straining (grain-grain contacts and small pore throats), size exclusion, ripening, bridging, clogging and attachment on nanoscale surface heterogeneity [8,20,36, 44,45].

Recently modeling studies have been performed to simulate the deposition of colloids in porous media by incorporating mechanisms such as mechanical filtration and straining to predict colloid behavior obtained from column experiments [22,24,25,46,47]. However, discrepancies between modeling and column experiments were observed due to the use of simplified assumptions and lack of incorporating mechanisms that take place at the pore-scale. Therefore, direct visualization studies are essential to understand and accurately model pore-scale mechanisms of colloid deposition and release.

Some studies implemented real-time, pore-scale visualization of colloid release experiments were conducted using an impinging jet to study the influence of colloid type, surface chemistry and surface roughness on colloid release from a flat surface [23,47]. Other attempts used flow cells containing glass beads equipped with visualization techniques to investigate the impact of colloid size on release upon perturbation of ionic strength and flow [48]. Some investigators used simplified geometry of micromodels to study the impact of different factors such as colloid size, shape, concentration, flow velocity, ionic strength on colloid transport and retention [49–52]. Although colloid-collector interactions at different conditions were revealed in these experiments, the use of simplified geometry was a limiting factor that prevented direct comparison to pore-scale processes in natural complex porous media systems. For instance, the spatial distribution of hydrodynamic forces due to pore-scale velocity distributions was not considered in the impinging jet experiments, although such distributions significantly influence colloid release in natural porous media systems [16,36].

The effects of attached colloid concentration and surface roughness on colloid release due to ionic strength reduction in sand columns were also investigated [53]. Although final colloid distribution patterns were obtained using scanning electron microscope after completion of the experiments [e.g., 53], real-time visualizations that reveal the dynamics of colloid deposition and release, reversible colloid attachment and re-deposition of released colloids were not observed.

As can be seen from studies listed above, colloid deposition and release mechanisms that occur due to perturbations in hydro-chemical condition were not observed at the pore-scale. Although some studies used direct visualization techniques, the use of simplified geometries of porous media prevents actual representation and capture of true mechanisms that take place in complex geometries of natural systems. Moreover, the impact of interaction favorability of colloids under transient hydro-chemical conditions was not tackled in previous studies.

The main objective of this study was to investigate, at the pore-scale,

Table 1
Summary of experimental conditions used in this study.

| Exp. ID	Colloids	Colloid favorability with the collector	Initial IS (mM of NaCl)	Zeta Potential (mV)	Transient Conditions		
					Flow perturbation (μL/min)	Solution chemistry	
						DI	pH 11
AMPS	AMPS	Favorable	0	20.2	10 and 100	–	✓
CMPS	CMPS	Medium-Favorable	0	−15.2	10 and 100	–	✓
PS_DI		Unfavorable	0	−63.8	10 and 100	–	✓
PS_10mM	PS	Unfavorable with medium IS	10	−51.8	10 and 100	✓	✓
PS_100 mM		Unfavorable with higher IS	100	−21.7	10 and 100	✓	✓
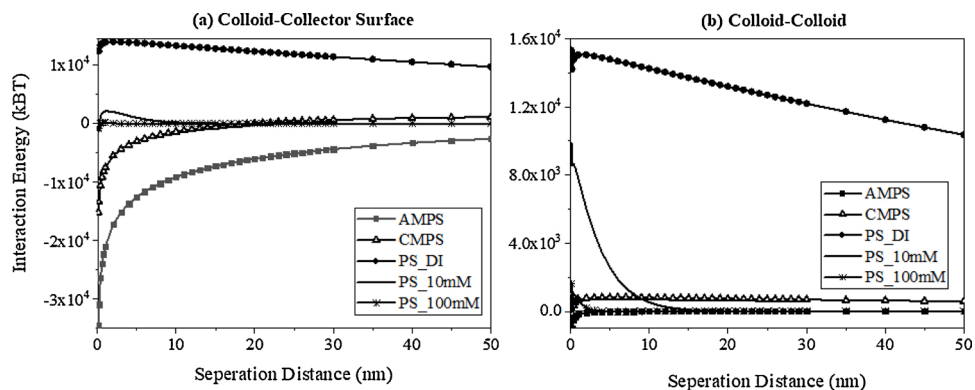
Fig. 1. DLVO energy profiles for various colloids interacting with (a) the collector surface, and (b) other colloids.
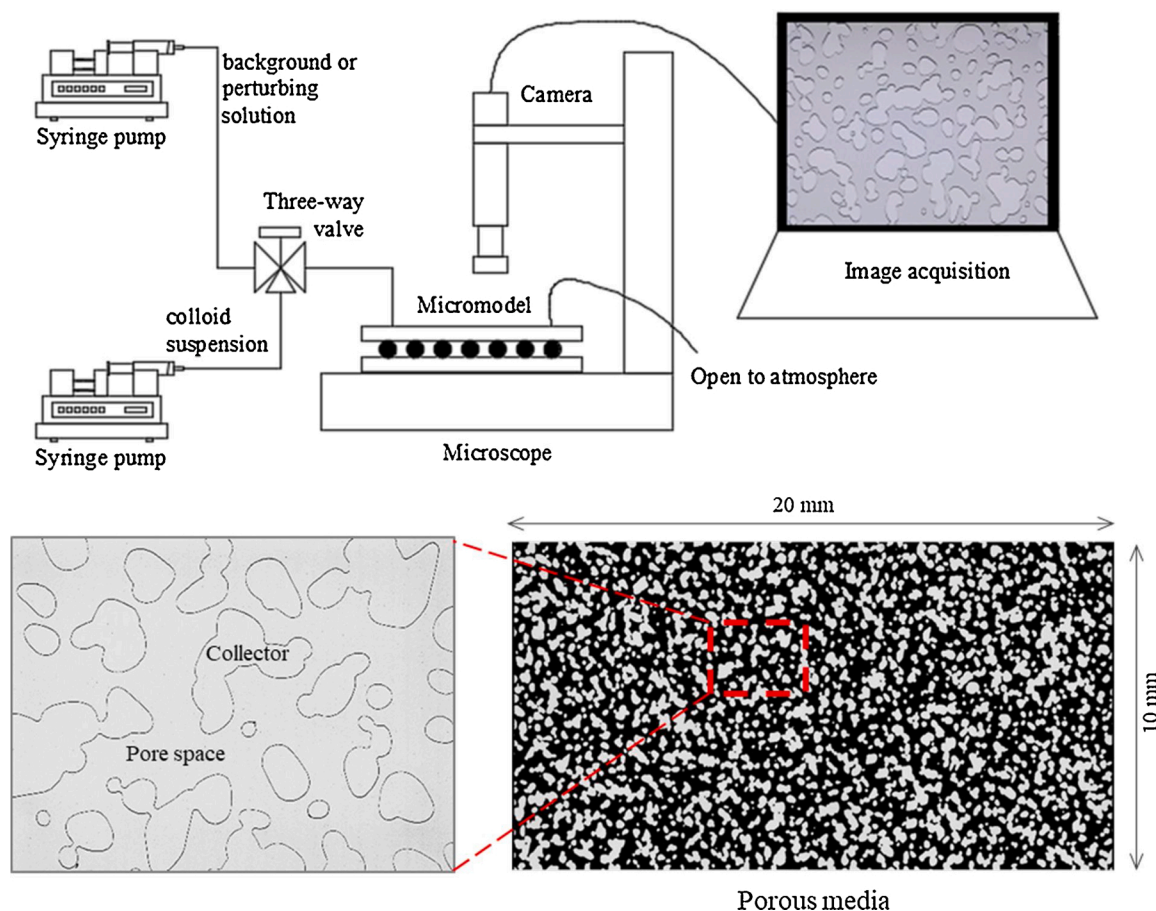

Fig. 2. Experimental setup of the micromodel used for colloid deposition and release experiments.

the impact of colloid interaction favorability on colloid deposition and subsequent release in response to perturbations of flow rate and solution chemistry in saturated porous media. Pore-scale experiments were conducted using a micromodel with physically representative geometry that represents natural porous media. Direct pore-scale images were obtained at different stages of colloid deposition and release to visualize and quantify colloids deposition and release mechanisms in the pore-space of the micromodel. Favorable, medium-favorable and unfavorable colloids were used in the experiments. Colloids were deposited in the micromodel and then a series of colloids release experiments were conducted at different conditions including increasing the flow rate, decreasing the ionic strength and increasing the solution pH.

2. Materials and methods

2.1. Colloids characteristics

Polystyrene (PS), carboxylate-modified polystyrene (CMPS), and aminate-modified polystyrene (AMPS) microspheres (Magsphere Inc., Pasadena, CA) were used as the colloids in this study. All colloids have a similar diameter and density of 5 μm and 1.05 g/cc, respectively. Zeta potential values were measured using Zetasizer (Nano ZSP, Malvern Panalytical, Southborough, MA) at 21 °C for the colloids in their respective background solution and the results are given in Table 1. Fig. 1 shows the computed DLVO energy profiles of colloid interactions with surfaces of the micromodel and other colloids (See supplementary material for a detailed description of DLVO energy calculations). As inferred from the energy profiles given in Fig. 1-a, three different favorability of interactions with the micromodel were shown by the colloids used in this study. These interactions were favorable, medium-favorable and unfavorable for AMPS, CMPS, and PS colloids, respectively.

A 10 % stock colloid solution was diluted using a background solution to obtain a final concentration of 2.9×10^7 colloids/mL to prevent inlet clogging of the micromodel. The diluted colloid suspensions were sonicated in a water bath for 30 min prior to the injection into the micromodel using an ultrasonic processor (SONICS, Vibra cell) to uniformly disperse the colloids in the background solution.

2.2. Background solutions

Background solutions for each experimental condition were prepared by dissolving sodium chloride (NaCl) in deionized water (DI) to obtain different ionic strengths used in the experiments as shown in Table 1. The pH for all solutions was maintained as 6.3 (i.e., the pH of deionized water) by adding drops of 0.1 M of sodium hydroxide (NaOH) solution. Three different ionic strengths (i.e., 0, 10, and 100 mM of NaCl, low, medium and high ionic strength) were selected to investigate the impact of ionic strength on colloid deposition and release mechanisms for unfavorable colloids (i.e., PS colloids).

2.3. Porous media

A micromodel fixed on a borosilicate glass with a total area of 20 mm × 10 mm and a depth of 20 μm (Micronit Micro Technologies B.V., Enschede, Netherlands) was used as the porous medium with a porosity of 0.58 and pore-volume of 2.3 μL. The inlet port of the micromodel was connected to a syringe pump (Kats Scientific, NE-1010) using a Teflon tube as shown in Fig. 2. The micromodel was cleaned before the start of every experiment by injecting 100 pore volumes (PVs) of ethanol followed by 500 PVs of deionized water. The micromodel was then dried in an oven at a temperature of 80 °C for 48 h.

2.4. Experimental procedure

Fig. 2 shows the experimental setup used in this study. It is mainly composed of a glass micromodel, syringe pumps, and a microscope (Leica Z6 APO) equipped with a high-resolution camera (Leica MC170 with a resolution of 5 Mpixels). The oven-dried micromodel was placed on the microscope stage and then connected to precision syringe pumps via a three-way valve using Teflon tubes. Air-bubbles in the micromodel were displaced or dissolved by injecting several PVs of deionized water.
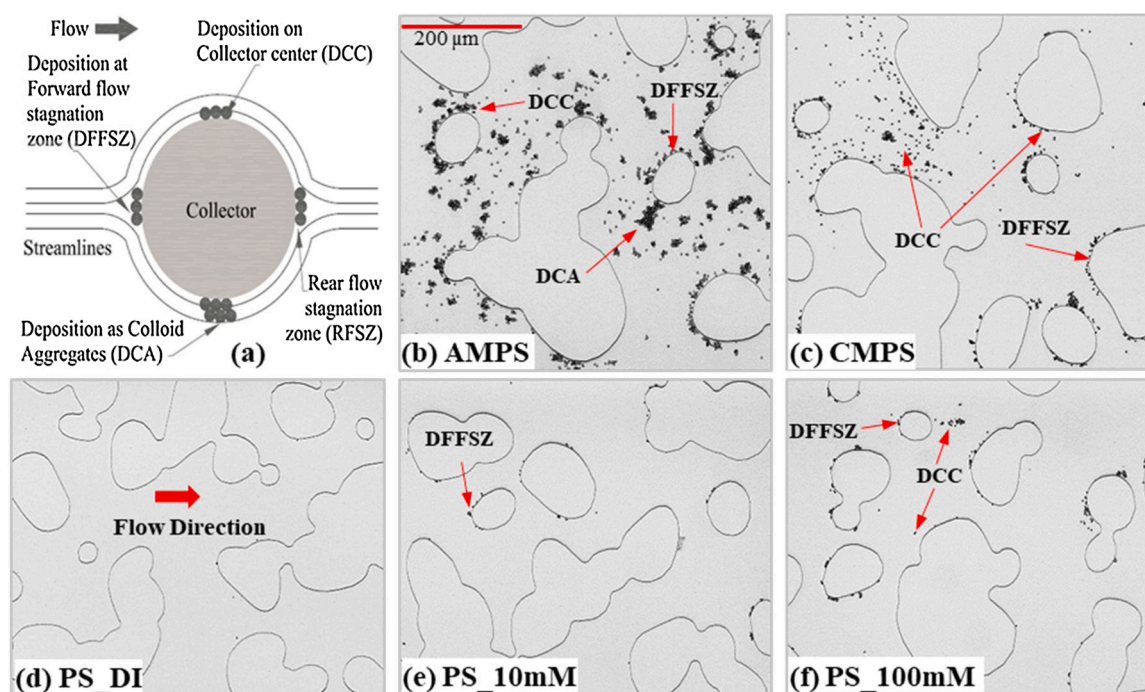

Fig. 3. (a) Schematic of possible colloid deposition mechanisms on a collector surface; i.e., DCC, DFFSZ, and DCA; Colloid deposition mechanisms observed for (b) the AMPS system (favorable colloids); (b) the CMPS system (medium-favorable colloids); (d) the PS_DI system (unfavorable colloids); (e) the PS_10mM system (unfavorable colloids with medium ionic strength); and (f) the PS_100 mM system (unfavorable colloids with high ionic strength).

Before injecting the colloid suspension, the micromodel was equilibrated by injecting 100 PVs of colloid-free background solution at the same flow rate that was used during colloid deposition and release experiments. The colloid suspension was then injected at 5 µL/min (mean pore water velocity of 36 m/d) for 30 PVs. This flow rate was chosen to prevent the settlement of particles in the injection syringe and to prevent clogging at the inlet of the micromodel. Colloid injection was followed by flushing colloid-free background solution to remove free colloids in the pore space of the micromodel (i.e., undeposited colloids). Upon flushing the micromodel with a colloid-free background solution, only the deposited colloids remained in the micromodel, which is designated as the deposition phase in this study. Pore-scale images were captured at different locations of the deposition phase to visually identify colloid deposition mechanisms and patterns under different favourability of colloids.

Once the deposition phase was established, the colloid release was investigated under the following perturbation conditions: (1) increase the flow rate without changing chemical conditions (i.e., background solution injection at flow rates of 10 µL/min and 100 µL/min, which is 2× and 20× of the colloid deposition flow rate); (2) reduction of ionic strength to 0 mM NaCl at a constant flow rate (i.e., deionized water injection at 5 µL/min); and (3) increase of solution pH to pH 11 at a constant flow rate (i.e., 1 mM NaOH solution injection at 5 µL/min). A summary of the experimental conditions used in this study is given in Table 1. Each experiment was repeated twice to ensure the reliability of the obtained results.

2.5. Image processing

The optical microscope and high-resolution camera were used to capture pore-scale images of colloid deposition and release in the micromodel. During the experiments, images were acquired at the deposition phase and at different perturbation phases using 2.5× magnification with a 2× plan apochromatic objective (0.234 numerical aperture, and 0.94 µm/pixel resolution) which was sufficient to resolve individual colloids. For each experimental condition, a series of images were captured with sufficient overlap and were registered to obtain a large image at the central region of the micromodel of an area of 4.7 × 18.9 mm². A precise moving controller was used for horizontal and vertical movement of the micromodel at each phase of the experiment.

The quantity of colloids retained in the micromodel at each experimental condition was computed from the respective captured images and presented as a percentage of the pore space. To identify deposited colloids in a given image (i.e., segment images), the image at a given experimental condition was subtracted from a mask (i.e., an image of water-saturated micromodel). A median filter was applied to remove possible noise due to contrast variations at the boundaries of different phases in images. Pixels corresponding to colloids were identified from the segmented image by pixel counting and then the percentage of colloids retained at each experimental condition was estimated.

3. Results and discussions

3.1. Effect of favorability of interaction on colloid deposition mechanisms

Three mechanisms of colloid deposition in saturated porous media as a function of colloid favorability were visually observed in this study. These mechanisms include (1) Deposition on Collector Center where the flow streamlines are parallel to the collector surface (DCC), (2) Deposition in Forward Flow Stagnation Zone (DFFSZ), and (3) Deposition as Colloid Aggregates (DCA).

Fig. 3 shows pore-scale images of size 1.0 mm × 1.0 mm (1064 × 1064 pixels) obtained for different experimental conditions investigated in this study to visually identify mechanisms of colloid deposition in saturated porous media. As shown in Fig. 3-a, DCC takes place at locations on a collector surface where the velocity of flow is highest.

Table 2
Summary of observed deposition mechanisms on a collector surface for different types of colloids.

Exp. ID	Colloid favorability with the collector	The intensity of colloid deposition mechanism for		
		Deposition on Collector Center (DCC)	Deposition in Forward Flow Stagnation Zone (DFFSZ)	Deposition as Colloid Aggregates (DCA)
AMPS	Favorable	Very High	Very High	Very High
CMPS	Medium-Favorable	High	Very High	Medium
PS_DI	Unfavorable	None	None	None
PS_10mM	Unfavorable with medium IS	Very Low	High	Very Low
PS_100 mM	Unfavorable with higher IS	Low	Very High	Low

Whereas DFFSZ takes place at locations where the local flow velocity is zero near the collector. DCA occurs for colloids when colloid-colloid interactions are attractive. Surfaces of the top and the bottom of the micromodel can be considered as a collector center as the flow velocity is relatively high. Table 2 summarizes the intensity of colloid deposition mechanisms for different types of colloids as a function of favorability of interaction as revealed from pore-scale images obtained in this study.

CFT predicts that the DCC mechanism occurs via interception when colloids travel along streamlines of flow. The superior adhesion force between the colloid and collector surface overcome hydrodynamic forces which in turn leads to colloid attachment on the collector center via interception. However, the DFFSZ mechanism takes place when colloids are trapped in the forward flow stagnation zones (FFSZ) due to the attractive interaction energy between colloids and collector surface regardless of the separation distance. At these conditions, deposition of colloids occurs since the hydrodynamic forces at the stagnation zones are negligible to prevent the attachment of colloids.

As observed from pore-scale images and reported in Table 2, the intensity of DCC decreases as the favorability of colloids decreases and as the ionic strength decrease for unfavorable colloids. High hydrodynamic resisting forces on the collector center reduce colloid attachment as colloid favorability and ionic strength decreases. However, Forward Flow Stagnation Zones (FFSZs) are active retention sites for colloids that exhibit attractive interaction energy where hydrodynamic forces are negligible. Moreover, under favorable colloid-colloid interaction conditions, a colloid in the bulk solution is attracted simultaneously by the collector surface and the deposited colloids resulting in DCA. As reported in Table 2, the intensity of the DCA mechanism varies for different colloids due to changes in the colloid-colloid interaction energy profiles as shown in Fig. 1-b.

AMPS colloids exhibited three types of deposition mechanisms (i.e., DCC, DFFSZ, and DCA) extensively as observed in Fig. 3-b and reported in Table 2. As shown in Fig. 1, the attractive interaction energy of AMPS colloids with the micromodel surface and other AMPS colloids explains the extensive deposition of colloids by DCC, DCA, and DFFSZ mechanisms. On the other hand, the deposition of CMPS colloids exhibited relatively less intensity of DCC and DCA mechanisms compared to AMPS colloids. As shown in Fig. 1-a, the presence of a slight energy barrier for CMPS colloids beyond a separation distance of 20 nm, allows the deposition of colloids that interact only within a separation distance less than 20 nm. Similarly, colloid-colloid interaction was also unfavorable for CMPS colloids beyond a separation distance of 0.2 nm due to the existence of a repulsive energy barrier. Therefore, for CMPS colloids, the frequency of DCC and DCA mechanisms was less than what was observed for AMPS colloids as observed in Fig. 3-c and reported in Table 2.

Moreover, pore-scale images obtained in this study show that significant DCC occurs near small pores as shown in Fig. 3-b and -c. As a
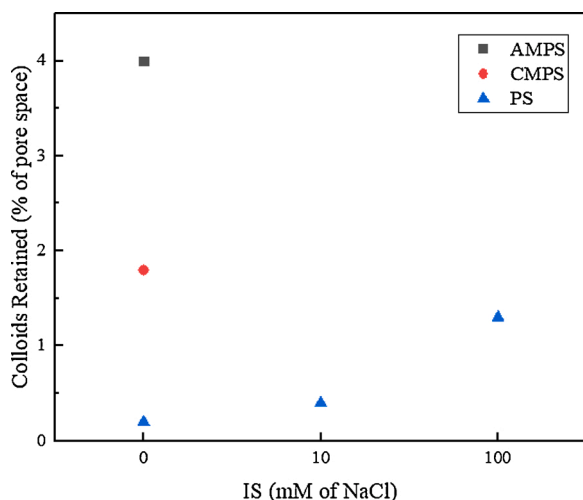
Fig. 4. Impact of favourbility of collodis on their deposition: Colloids retained in the micromodel as a percentage of the pore space at flow rate = 5 μL/min and pH = 6.3 (i.e., deposition phase).

large number of colloids follow the shortest paths in the pore space (i.e., higher flow velocity at small pores), a large number of colloids becomes available to interact with the collector center at small pores. Therefore, colloid deposition and subsequent ripening at small pores near the inlet would block or clog the pore space for favorable and medium-favorable colloids as revealed from this study.

As can be seen in Fig. 3-d, pore-scale images reveal that none of the deposition mechanisms were observed for unfavorable colloids (i.e., PS_DI). The absence of the attractive interaction energy between colloids and micromodel surfaces prevented the deposition of colloids by any deposition mechanism (including DFFSZ). Due to the lack of attractive energies, colloids that were transported towards FFSZ were relocated to the main flow stream along the collector surface and then transported through the pore-space without any retention. However, as ionic strength increases, PS colloids exhibit intensive deposition via different mechanisms as shown in Figs. 3-e and f (i.e., PS_10mM and PS_100 mM). At medium and higher ionic strength, DFFSZ was dominant over DCC and DCA for unfavorable colloids (Table 2). This is mainly due to the insignificant hydrodynamic forces in the FFSZ compared to the adhesion forces that exist at a very short separation distance as explained in previous theoretical studies [29]. Nevertheless, the intensity of DCC, DFFSZ, and DCA was higher for PS_100 mM compared to PS_10mM colloids. As seen in Fig. 1, as ionic strength increases, the repulsive energy barrier for unfavorable colloids decreases and the separation distance at which the primary minimum occurs increases. Therefore, colloid interaction with the collector surface and other colloids at higher ionic strength (i.e., PS_100 mM) are more frequent than interactions at lower ionic strength (i.e., PS_10mM).

No individual colloid entrapment in small pore throats and grain-grain contacts was observed in any of the cases investigated in this study as the colloid size was small relative to the pore-throat size. Moreover, colloid deposition on Rear Flow Stagnation Zones (RFSZ) was not observed in pore-scale images obtained in this study which contradicts previous studies that suggested that colloid deposition occurs in FFSZ and RFSZ under unfavorable conditions as fluid drag forces are absent or negligible [16,29]. Moreover, other studies suggested that fluid drag and shear might translate particles that are trapped in a secondary minimum until they reach RFSZ [54]. However, in this study, pore-scale images show that colloids retained via secondary minimum on the collector center were not translated to RFSZ as hypothesized in previous studies, they rather moved to the bulk solution or remained attached on the collector center (e.g., Fig. 3-a). The nanoscale roughness on the collector surface imparted a vital role to prevent the translocation

of deposited colloids along the collector surface in contrast to the theoretical studies.

Percentages of colloids retained in the micromodel as a percentage of the pore-space at the end of the deposition phase of each experimental condition were determined by processing the acquired images as shown in Fig. 4. Percentages of colloids retained in the pore-space show a clear trend of the deposition increase with the favorability of interaction as well as the increase in ionic strength for unfavorable conditions as can be seen in Fig. 4. Thus, a greater deposition was observed for AMPS (i.e., 4 % of pore-space) compared to CMPS colloids (i.e., 1.8 % of the pore-space). Although PS_DI colloids show a repulsive interaction profile (Fig. 1-a), deposition of 0.2 % of colloids was observed on the nanoscale surface heterogeneities as reported in previous studies [20,47,55].

3.2. Colloid release by flow perturbations

Upon deposition of colloids in the micromodel, a stepwise increase of flow rate was applied to investigate the effect of perturbations of hydrodynamic forces on colloid release. The flow rate was increased by 2× and 20× the injected flow rate used to establish the deposition phase. Fig. 5 shows pore-scale images of size 1.2 mm × 1.0 mm (1276 × 1064 pixels) at the end of the deposition phase and at each velocity perturbation (i.e., 2× and 20× the flow rate used to establish the deposition stage). Fig. 6 shows fractions of colloids that remained in the micromodel as obtained from pore-scale images upon velocity changes. Table 3 summarizes colloid release behavior during transient conditions for different colloids as perceived from Figs. 5 and 6.

As shown in Fig. 5 and reported in Table 3, no significant colloid release from the micromodel was observed when the flow rate was increased to 2× for all experimental conditions. However, different colloid release patterns were observed when the flow rate was increased to a 20× injected flow rate. Upon a 20× increase in flow rate, the trend of colloid release followed a similar trend observed for colloid deposition mechanism, DCC, as reported in Table 2. Pore-scale images in Fig. 5 show that colloids that were subjected to release were initially deposited on the collector center in all the experimental conditions. The alteration of force balance acting on the deposited colloids due to a 20× increase in flow rate led to their release. In other words, due to flow perturbation, the hydrodynamic forces on the collector center are much higher than in FFSZs. Therefore, the spatial distribution of the deposited colloids and variations in hydrodynamic forces due to the pore structure were the major factors affecting the fractional colloid release in the porous media upon flow perturbations. Therefore, the negligible increase in hydrodynamic shear upon 2× increase in flow rate led to insignificant release of colloids at this flow rate as can be seen from Fig. 5 and Fig. 6. As shown in Fig. 5-e, an extensive release of unfavorable colloids was observed at high ionic strength (i.e., PS_100 mM). This observation contradicts previous studies that suggested that unfavorable colloids that were initially retained via secondary minimum under low ionic strength were released at high rates compared to colloids at high ionic strength as they were deposited permanently in deep energy well [20, 47,55].

As seen in Fig. 6, the AMPS colloid fraction retained in the micromodel after 20× perturbation increased to 10 % of the initially deposited colloids. This observation can be explained based on direct visual observation obtained from pore-scale images (e.g., Fig. 5-a). AMPS colloids were initially deposited as multi-layered aggregates which were redistributed to mono-layer aggregates upon the increase of flow rate to 20× the initial flow rate. Therefore, the percentage of initially deposited colloids estimated at the end of the deposition phase by image processing was underestimated due to the formation of multi-layered aggregates. Images also show that colloid aggregates aligned along the flow streamlines as a result of fluid drag forces acting on colloid clusters. Although the percentage of colloids retained after the flow perturbation (i.e., 20×) was estimated from the mono-layered aggregates, the colloid fraction retained after the flow perturbations did not show the actual
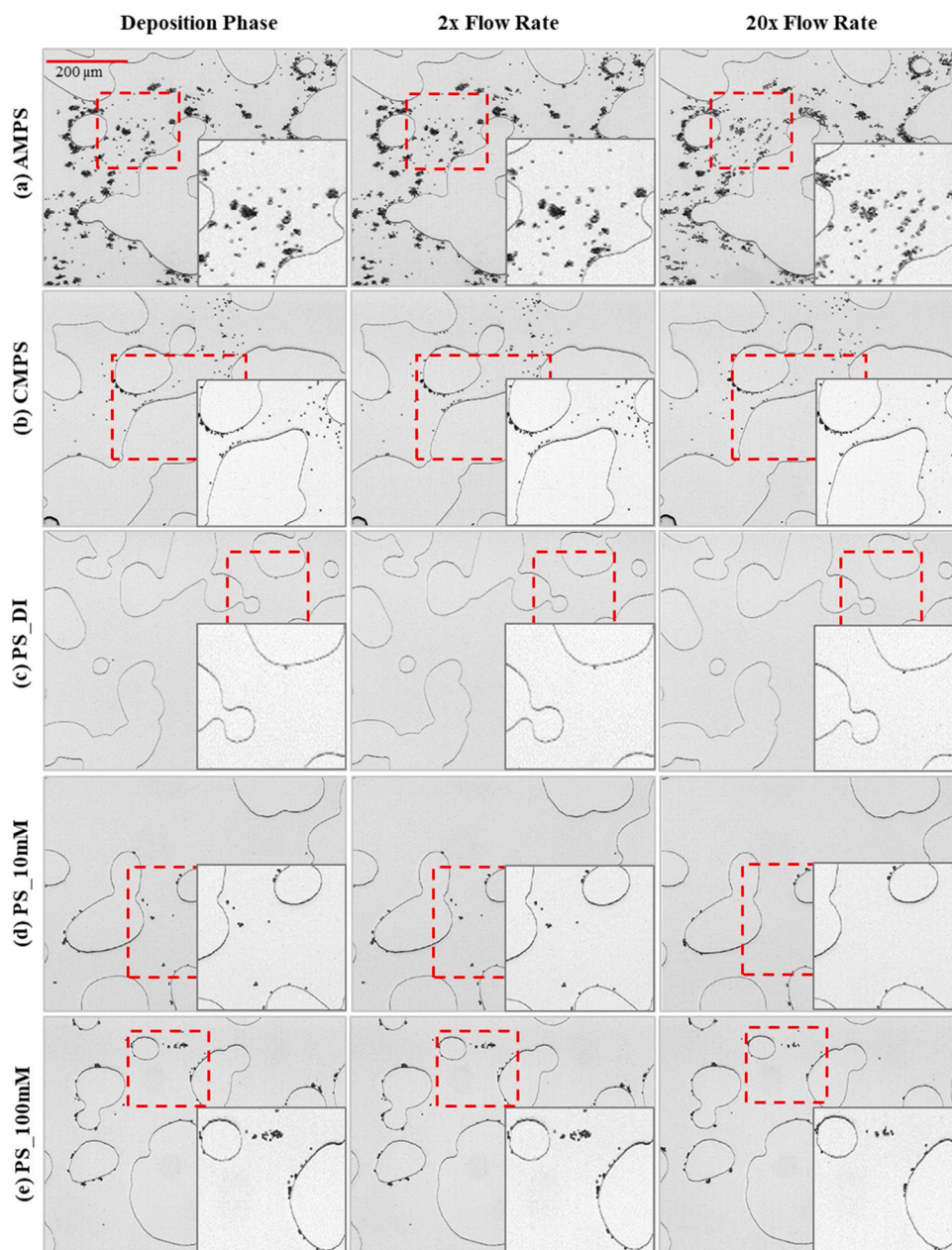
Fig. 5. Pore-scale images before and after perturbation of the flow rate for the experimental conditions used in this study.

behavior of AMPS colloids. Pore-scale images given in Fig. 5-a show an extensive release of AMPS colloids from the multi-layer colloid aggregates which were formed at the deposition phase and turned into a single layer of colloids.

As reported in Fig. 6, approximately 30 % of CMPS colloids that were deposited during the deposition phase were released upon the 20× increase in the flow rate (i.e., 100 μL/min). It was also observed that colloid release was insignificant for unfavorable colloids in deionized water (i.e., PS_DI). However, colloid release increased as solution ionic strength increased. It was observed that approximately 10 % and 20 % of colloids that were deposited at the deposition phase were released when the ionic strength of the solution increased to 10 mM and 100 mM, respectively (i.e., systems PS_10mM and PS_100 mM in Fig. 6).

Findings from this study revealed that the impact of spatial distribution of hydrodynamic forces on the behavior of colloid release was reasonably important asthe strength of colloid adhesive forces (i.e., interaction energies). In other words, colloids deposited on collector centers were more susceptible to release as compared to colloids

deposited in FFSZs. Besides the retention in FFSZ, colloid deposition on the collector center increased as the solution ionic strength for PS colloids increased as observed in Fig. 3-e, f, and reported in Table 2. Therefore, colloids at high ionic strength were released from collector centers upon a 20× increase in flow rate regardless of their adhesive forces which contradict previous studies [20,47,55]. Furthermore, the release of PS_DI colloids was not observed in this study even after a 20× increase in the flow rate. Deposition of approximately 0.2 % of the PS colloids under repulsive conditions (i.e., PS_DI) took place on low flow zones or surface heterogeneities (Fig. 5-c). Therefore, hydrodynamic forces imposed under the experimental conditions were not sufficient to release the deposited colloids back to bulk water.

3.3. Colloid release by perturbations in solution chemistry

The impact of perturbations in solution chemistry was investigated at two conditions: decreasing the solution ionic strength to 0 mM and increasing the solution pH to 11. Colloid release by the reduction in ionic
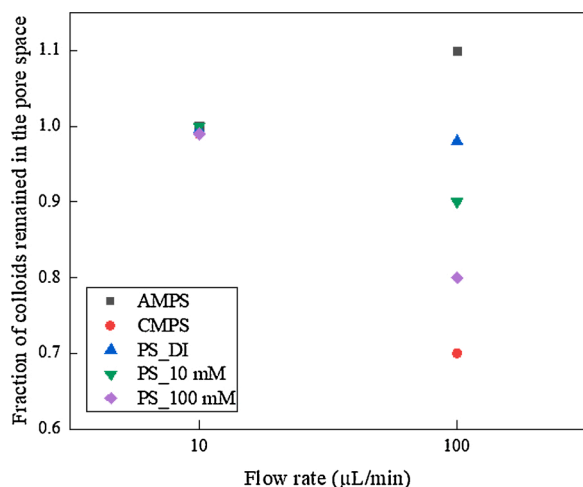
Fig. 6. Impact of flow perturbation on the release of colloids: the fraction of colloids remaining in the micromodel upon the increase of flow rate from 5 μL/min to 10 and 100 μL/min (2× and 20× the injection flow rate used to create the deposition phase of colloids).

Table 3
Summary of observed colloid release behavior in a saturated porous media for different types of colloids.

Exp. ID	Colloid favorability with the collector	Colloid release by perturbation in			
		Flow rate		Solution chemistry	
		2×	20×	Reduction in IS (0 mM)	Increase in pH (11)
AMPS	Favorable	None	Very High	–	Very High
CMPS	Medium-Favorable	None	High	–	High
PS_DI	Unfavorable	None	None	–	None
PS_10mM	Unfavorable with medium IS	None	Very Low	Very Low	Very Low
PS_100 mM	Unfavorable with higher IS	None	Low	Low	Low

strength was established only for unfavorable colloids (i.e., PS_10mM and PS_100 mM). Colloid injection at high ionic strength for favorable and medium-favorable colloids (i.e., AMPS and CMPS colloids, respectively) was difficult to achieve as it led to clogging the inlet of the micromodel. However, an increase in the pH of solutions was applied to all the experimental conditions in this study.

Pore-scale images in Fig. 7 show the colloids retained at the end of the deposition phase and upon reduction of ionic strength to 0 mM for unfavorable colloids (i.e., PS_10mM and PS_100 mM). As indicated in the red circles shown in Fig. 7, a high release of PS_100 mM colloids was observed. As observed from several pore-scale images captured, the released colloids at both ionic strength conditions were initially deposited on the collector center (i.e., DCC) and a significant fraction of unmobilized colloids upon the decrease of the ionic strength was retained in FFSZ.

Fig. 8 shows pore-scale images before and after the increase of the pH of the solution for all types of colloids used in this study. For favorable and medium-favorable colloids (i.e., AMPS and CMPS as shown in Figs. 8-a and b), it was observed that colloids that were initially deposited on the collector centers (i.e., DCC) were released whereas a few of these colloids redeposited in the FFSZs.

The unfavorable colloids (i.e., PS_DI) deposited on nano-scale surface heterogeneities were not susceptible to release as observed in Fig. 8-c. However, as ionic strength increased, unfavorable colloids exhibited

colloid release from collector centers as shown in red circles in Figs. 8-d and f. As can be seen from the pore-scale images, the greater colloid release was observed for high ionic strength (i.e., PS_100 mM) than medium ionic strength conditions (i.e., PS_10mM) upon reduction in ionic strength to 0 mM. This can be attributed to considerable colloid DCC at high ionic strength compared to medium ionic strength conditions (Table 2).

Fig. 9 shows fractions of colloids that remained in the pore space upon the reduction of solution ionic strength and increase of solution pH. Table 3 summarizes the effect of colloid favorability and solution ionic strength on the release behavior of colloids. As shown in Fig. 9, a substantial release of deposited AMPS and CMPS colloids was observed due to the increase of the pH of the solution. Approximately, 70 % of AMPS and 58 % of CMPS colloids were mobilized upon the increase of solution pH. However, the release of unfavorable colloids (PS_DI) was negligible where less than 0.5 % of deposited colloids were released due to the pH increase. It was also observed from Fig. 9 that reduction of ionic strength led to the release of 8 % and 3 % of the initially deposited colloids of the PS_100 mM and PS_10mM colloids, respectively.

Previous studies reported that the unfavorable colloids attached via secondary minimum were released upon the reduction of ionic strength since the secondary minima vanish at low ionic strength [20,31,47]. As observed in Fig. 1, as the ionic strength decreases from 100 mM to 10 mM, the energy barrier increases and the secondary minimum decreases. Therefore, at an ionic strength of 100 mM, collector surfaces were favorable for secondary minimum attachment. On the other hand, at an ionic strength of 10 mM, the deposited colloids may move back to the bulk water due to the shallow energy well (−2 kBT) and high drag forces on collector centers. Nevertheless, the release of colloids deposited in FFSZs (i.e., DFFSZ) was not observed in this study under both ionic strength conditions. This observation can be explained by two possible reasons. Firstly, the hydrodynamic drag forces acting on the colloids in FFSZ were not sufficient to release colloids back to the bulk solution [29]. Secondly, colloids deposited in the secondary minimum overcome the energy barrier and translated to the primary minimum (due to the absence of re-entraining forces in FFSZ) where the primary minimum exists at shorter separation distances at both ionic strength conditions (i.e., 0.2 nm, Fig. 1-a). The release of colloids from the primary minimum was not observed by the reduction in ionic strength as the attachment occurs at deep energy well.

The observed behavior of colloid release from the micromodel upon pH increase can be related to zeta potential values and DLVO energy profiles. Zeta potential values of AMPS, CMPS, and PS colloids at pH of 11 were measured as −14, −25, and −72 mV, respectively. The corresponding DLVO curves are shown in Fig. 10. As shown in Table 1, zeta potential values of colloids decreased as the pH of the solution increased; colloids develop stronger negative surface charges resulted from the OH⁻ ions of the bulk solution [56,57]. Consequently, the enhanced colloid release for the AMPS colloids with the increase in solution pH took place due to the conversion of surface charge from positive to negative. However, it was observed that about 30 % of the initially deposited colloids remained in the porous media. This observation suggests that retained colloids were deposited in a deep energy well at short separation distances (less than 3 nm) where the DLVO profiles show primary minimum interaction even after perturbation with high pH solution (Fig. 10). In other words, AMPS colloids deposited in the porous media at long-range of separation distances (i.e., more than 3 nm) were released back to the bulk solution during the perturbation phase due to repulsive interaction forces.

The release of CMPS colloids can be understood within the context of DLVO profiles. Colloids deposited within a separation distance less than 0.2 nm were retained in the micromodel despite the increase of the pH of the solution. Pore-scale images shown in Fig. 8 reveal that the released colloids for all cases were initially attached on the collector center and those colloids retained after the perturbation phase were deposited in FFSZ. This observation indicates that the retained colloids in FFSZ were
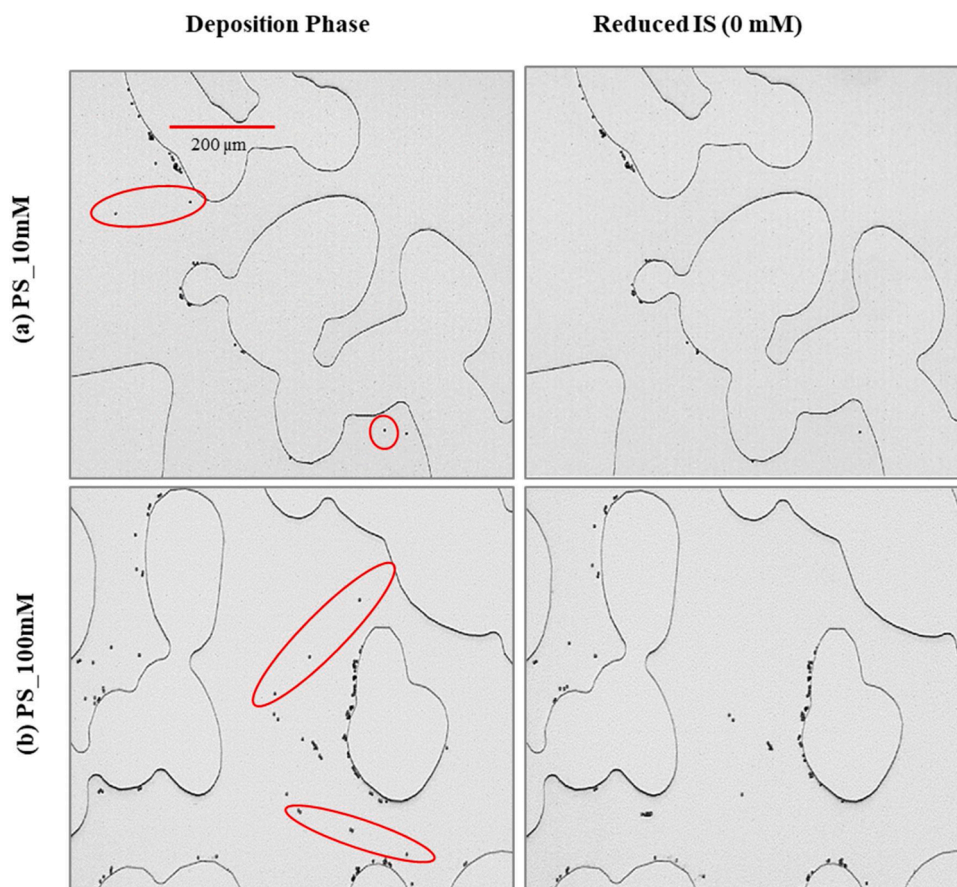
Deposition Phase   **Reduced IS (0 mM)**

Fig. 7. Pore-scale images at different stages of perturbation for PS_100 mM and PS_10mM conditions.

interacting in the primary minima at very short separation distances even under unfavorable conditions in this study as explained earlier (i. e., PS_10mM and PS_100 mM). Although previous studies suggest the release of colloids deposited initially in the primary minimum by increasing the solution pH [8,55,57,58], the observed colloid release in this study was insignificant for colloids attached in FFSZ. These findings suggest that the negligible drag forces acting in FFSZ and the greater energy barrier for release (due to deep primary minimum interaction) were the main factors that lead to the permanent retention of colloids in FFSZ. Generally, colloid release upon perturbations increased with an increase in interaction favorability as well as ionic strength for unfavorable colloids (Table 3).

4. Conclusions

This study elucidated the importance of understanding pore-scale deposition mechanisms of colloids to explain the colloid release behavior in saturated porous media during transient hydro-chemical conditions. Main findings obtained from this pore-scale visualization study are:

1 Three mechanisms of colloid deposition in saturated porous media as a function of colloid favorability were observed in this study: Deposition on Collector Center (DCC), Deposition in Forward Flow Stagnation Zones (DFFSZ), and Deposition as Colloid Aggregates (DCA).
2 Favorable colloids exhibited extensive DCC and DCA as adhesion forces overcome hydrodynamic forces. However, at medium and high ionic strength, DFFSZ was dominant over DCC and DCA for

unfavorable colloids as the hydrodynamic forces are negligible at FFSZ.
3 The intensity of deposition mechanisms decreased as the favorability of colloids decreased and as the ionic strength decreased for unfavorable colloids (i.e., greater deposition for favorable colloids and at higher ionic strength for unfavorable colloids).
4 Pore-scale images showed that, upon an increase of flow rate to 20× the initial flow rate, colloids that were initially deposited on collector centers were more susceptible to release as compared to colloids that were initially deposited in FFSZs. Perturbation in flow rate induced higher hydrodynamic forces on the collector center as compared to FFSZs.
5 The negligible increase in hydrodynamic shear upon a 2× increase in flow rate led to insignificant release of colloids. However, upon a 20× increase in flow rate, the trend of colloid release followed a similar trend observed for colloid deposition mechanism (i.e., DCC).
6 As observed from captured pore-scale images, the released colloids at all experimental conditions were initially deposited on the collector center (i.e., DCC) and a significant fraction of unmobilized colloids upon hydro-chemical perturbations was retained in FFSZ.
7 Significant colloid release took place for unfavorable colloids at high ionic strength due to greater colloid deposition on the collector center compared to medium ionic strength.
8 For favorable colloids, the presence of repulsive interaction for a long-range of separation distance at high pH induced the release of colloids deposited on the collector center upon an increase in solution pH. However, the retained colloids upon the perturbation phase were deposited in FFSZ at short separation distances where a deep primary minimum existed.
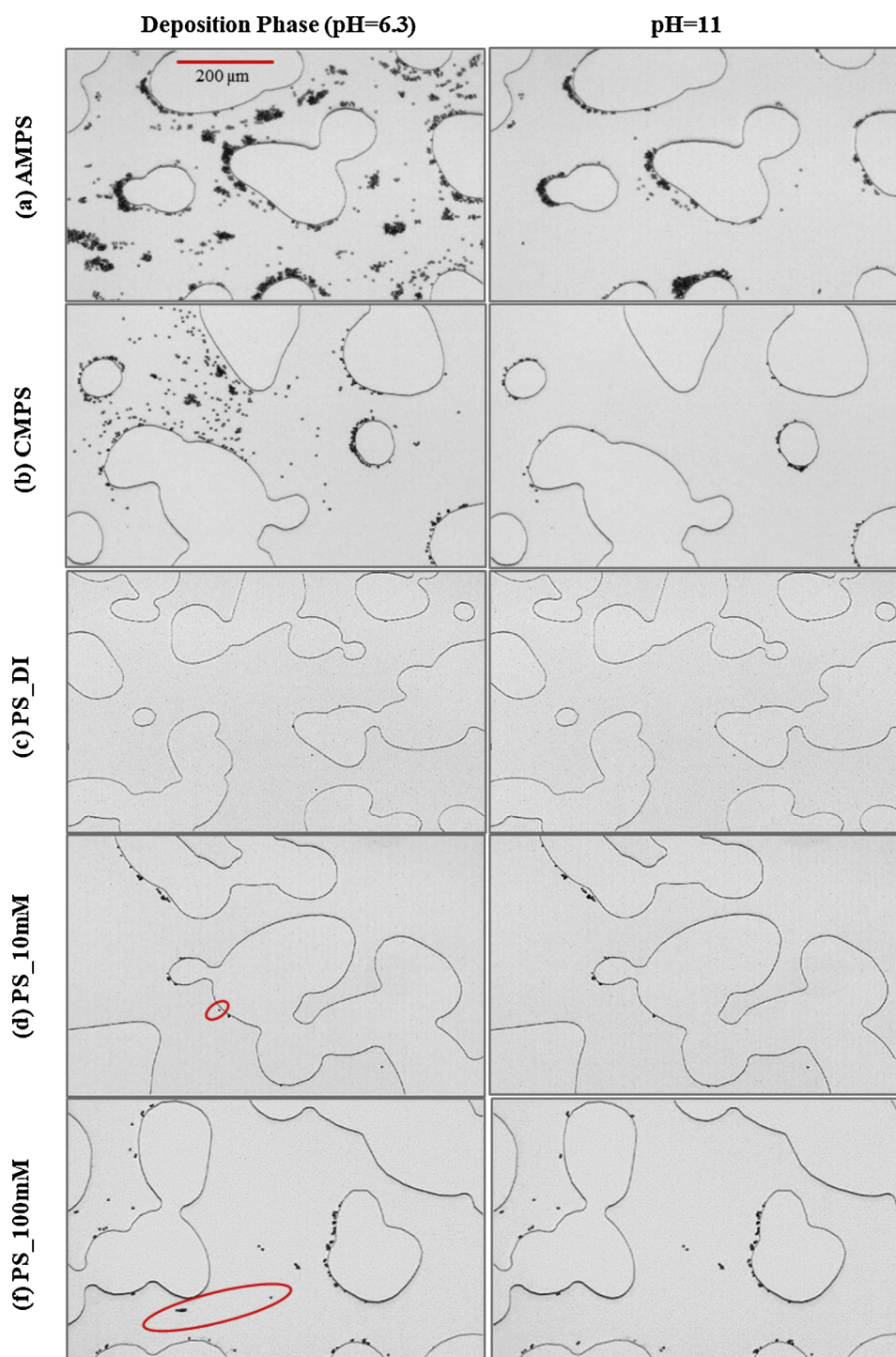
Deposition Phase (pH=6.3)   **pH=11**

Fig. 8. Pore-scale images after an increase in pH of the background solution (i.e., pH of 11) for AMPS, CMPS, and PD_DI colloids.

9 The negligible hydrodynamic drag forces in FFSZ and deep primary minimum interaction at short separation distances were the major factors that hindered the release of colloids in FFSZ under transient hydro-chemical conditions.

CRediT authorship contribution statement

Safna Nishad: Methodology, Validation, Investigation, Formal analysis, Writing - original draft. **Riyadh I. Al-Raoush:** Methodology, Conceptualization, Investigation, Supervision, Writing - review &

editing, Funding acquisition, Resources. **Motasem Y.D. Alazaiza:** Writing - review & editing.

Declaration of Competing Interest

The authors declare that they have no known competing financial interests or personal relationships that could have appeared to influence the work reported in this paper.
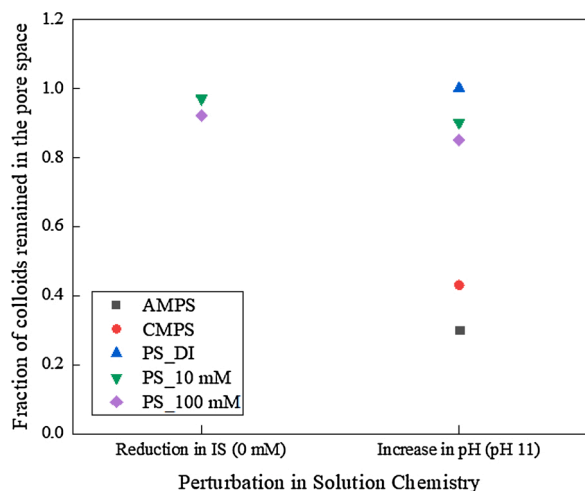
Fig. 9. Impact of ionic stength and pH perturbations on the release of colloids: fraction of colloids retained in the micromodel after perturbations in solution chemistry.
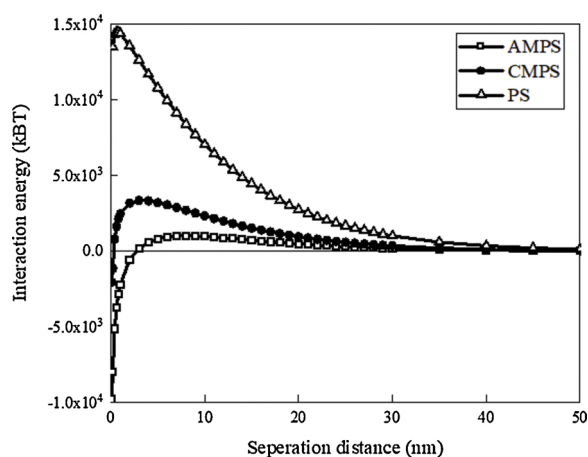

Fig. 10. DLVO energy profiles for different colloids interacting with the collector surface at pH 11.

Appendix A. Supplementary data

Supplementary material related to this article can be found, in the online version, at doi:https://doi.org/10.1016/j.colsurfa.2021.126188.

References

[1] A.N.D. Posadas, D. Giménez, M. Bittelli, C.M.P. Vaz, M. Flury, Multifractal characterization of soil particle-size distributions, Soil Sci. Soc. Am. J. 65 (2001) 1361–1367.

[2] M.A. Kiser, P. Westerhoff, T. Benn, Y. Wang, J. Perez-Rivera, K. Hristovski, Titanium nanomaterial removal and release from wastewater treatment plants, Environ. Sci. Technol. 43 (2009) 6757–6763.

[3] L.W. Canter, R.C. Knox, Septic Tank System Effects on Ground Water Quality, Lewis Publishers, Chelsea, MI, 1985.

[4] J.F. McCarthy, L.D. McKay, Colloid transport in the subsurface: past, present, and future challenges, Vadose Zone J. 3 (2004) 326–337.

[5] E. Rosenbrand, I.L. Fabricius, H. Yuan, Thermally induced permeability reduction due to particle migration in sandstones: the effect of temperature on kaolinite mobilisation and aggregation, in: Proc. Thirty-Seventh Work. Geotherm. Reserv. Eng. Stanford Univ. Stanford, California, Jan, 2012.

[6] T. Tosco, J. Bosch, R.U. Meckenstock, R. Sethi, Transport of ferrihydrite nanoparticles in saturated porous media: role of ionic strength and flow rate, Environ. Sci. Technol. 46 (2012) 4008–4015.

[7] I.L. Molnar, D.M. O'Carroll, J.I. Gerhard, Impact of surfactant-induced wettability alterations on DNAPL invasion in quartz and iron oxide-coated sand systems, J. Contam. Hydrol. 119 (2011) 1–12.

[8] R. Yuan, W. Zhang, X. Tao, S. Wang, L. Zhang, Coupled effects of high pH and chemical heterogeneity on colloid retention and release in saturated porous media, Colloids Surf. A Physicochem. Eng. Asp. 586 (2020), 124285.

[9] C. Yu, X. Guo, X. Gao, Z. Yu, J. Jiang, Transport of graphene quantum dots (GQDs) in saturated porous media, Colloids Surf. A Physicochem. Eng. Asp. 589 (2020), 124418.

[10] S. Sasidharan, S. Torkzaban, S.A. Bradford, P.J. Dillon, P.G. Cook, Coupled effects of hydrodynamic and solution chemistry on long-term nanoparticle transport and deposition in saturated porous media, Colloids Surf. A Physicochem. Eng. Asp. 457 (2014) 169–179.

[11] X. Jiang, M. Tong, R. Lu, H. Kim, Transport and deposition of ZnO nanoparticles in saturated porous media, Colloids Surf. A Physicochem. Eng. Asp. 401 (2012) 29–37.

[12] M. Gavrilescu, Colloid-mediated transport and the fate of contaminants in soils. Role Colloid. Syst. Environ. Prot., Elsevier, 2014, pp. 397–451.

[13] T. Hou, R. Xu, D. Tiwari, A. Zhao, Interaction between electrical double layers of soil colloids and Fe/Al oxides in suspensions, J. Colloid Interface Sci. 310 (2007) 670–674.

[14] N. Tufenkji, M. Elimelech, Deviation from the classical colloid filtration theory in the presence of repulsive DLVO interactions, Langmuir 20 (2004) 10818–10828.

[15] P.N. Mitropoulou, V.I. Syngouna, C.V. Chrysikopoulos, Transport of colloids in unsaturated packed columns: role of ionic strength and sand grain size, Chem. Eng. J. 232 (2013) 237–248, https://doi.org/10.1016/j.cej.2013.07.093.

[16] S.A. Bradford, S. Torkzaban, A. Wiegmann, Pore-scale simulations to determine the applied hydrodynamic torque and colloid immobilization, Vadose Zone J. 10 (2011) 252–261.

[17] Y. Liang, S.A. Bradford, J. Simunek, H. Vereecken, E. Klumpp, Sensitivity of the transport and retention of stabilized silver nanoparticles to physicochemical factors, Water Res. 47 (2013) 2572–2582.

[18] S.A. Bradford, S. Torkzaban, Determining parameters and mechanisms of colloid retention and release in porous media, Langmuir 31 (2015) 12096–12105.

[19] Y. Sun, B. Gao, S.A. Bradford, L. Wu, H. Chen, X. Shi, J. Wu, Transport, retention, and size perturbation of graphene oxide in saturated porous media: effects of input concentration and grain size, Water Res. 68 (2015) 24–33.

[20] S. Torkzaban, S.A. Bradford, J.L. Vanderzalm, B.M. Patterson, B. Harris, H. Prommer, Colloid release and clogging in porous media: effects of solution ionic strength and flow velocity, J. Contam. Hydrol. 181 (2015) 161–171.

[21] S.A. Bradford, H. Kim, Causes and implications of colloid and microorganism retention hysteresis, J. Contam. Hydrol. 138 (2012) 83–92.

[22] D. Grolimund, M. Borkovec, Release of colloidal particles in natural porous media by monovalent and divalent cations, J. Contam. Hydrol. 87 (2006) 155–175.

[23] E. Pazmino, J. Trauscht, B. Dame, W.P. Johnson, Power law size-distributed heterogeneity explains colloid retention on soda lime glass in the presence of energy barriers, Langmuir 30 (2014) 5412–5421.

[24] S.A. Bradford, F.J. Leij, Modeling the transport and retention of polydispersed colloidal suspensions in porous media, Chem. Eng. Sci. 192 (2018) 972–980.

[25] P.C. Sanematsu, K.E. Thompson, C.S. Willson, Pore-scale modeling of nanoparticle transport and retention in real porous materials, Comput. Geosci. 127 (2019) 65–74.

[26] J. Bergendahl, D. Grasso, Prediction of colloid detachment in a model porous media: hydrodynamics, Chem. Eng. Sci. 55 (2000) 1523–1532.

[27] C. Shen, B. Li, Y. Huang, Y. Jin, Kinetics of coupled primary-and secondary-minimum deposition of colloids under unfavorable chemical conditions, Environ. Sci. Technol. 41 (2007) 6976–6982.

[28] S.A. Bradford, S. Torkzaban, H. Kim, J. Simunek, Modeling colloid and microorganism transport and release with transients in solution ionic strength, Water Resour. Res. 48 (2012).

[29] S. Torkzaban, S.A. Bradford, S.L. Walker, Resolving the coupled effects of hydrodynamics and DLVO forces on colloid attachment in porous media, Langmuir 23 (2007) 9652–9660.

[30] C. Zhang, A. Yan, G. Wang, C. Jin, Y. Chen, C. Shen, Impact of flow velocity on transport of graphene oxide nanoparticles in saturated porous media, Vadose Zone J. 17 (2018).

[31] S. Torkzaban, S.S. Tazehkand, S.L. Walker, S.A. Bradford, Transport and fate of bacteria in porous media: coupled effects of chemical conditions and pore space geometry, Water Resour. Res. 44 (2008).

[32] M.W. Hahn, C.R. O'Melia, Deposition and reentrainment of Brownian particles in porous media under unfavorable chemical conditions: some concepts and applications, Environ. Sci. Technol. 38 (2004) 210–220.

[33] M.W. Hahn, D. Abadzic, C.R. O'Melia, Aquasols: On the role of secondary minima, Environ. Sci. Technol. 38 (2004) 5915–5924.

[34] B. Derjaguin, L. Landau, The theory of stability of highly charged lyophobic sols and coalescence of highly charged particles in electrolyte solutions, Acta Physicochim. URSS 14 (1941) 58.

[35] J.T.G. Overbeek, E.J.W. Verwey, Theory of the Stability of Lyophobic Colloids: the Interaction of Sol Particles Having an Electric Double Layer, 1948.

[36] C. Shen, V. Lazouskaya, H. Zhang, F. Wang, B. Li, Y. Jin, Y. Huang, Theoretical and experimental investigation of detachment of colloids from rough collector surfaces, Colloids Surfaces A Physicochem. Eng. Asp. 410 (2012) 98–110.

[37] S. Torkzaban, S.A. Bradford, J. Wan, T. Tokunaga, A. Masoudih, Release of quantum dot nanoparticles in porous media: role of cation exchange and aging time, Environ. Sci. Technol. 47 (2013) 11528–11536.

[38] S.A. Bradford, H. Kim, C. Shen, S. Sasidharan, J. Shang, Contributions of nanoscale roughness to anomalous colloid retention and stability behavior, Langmuir 33 (2017) 10094–10105.

[39] C. Shen, Y. Jin, J. Zhuang, T. Li, B. Xing, Role and importance of surface heterogeneities in transport of particles in saturated porous media, Crit. Rev. Environ. Sci. Technol. 50 (2020) 244–329.

[40] C. Shen, S.A. Bradford, T. Li, B. Li, Y. Huang, Can nanoscale surface charge heterogeneity really explain colloid detachment from primary minima upon reduction of solution ionic strength? J. Nanopart. Res. 20 (2018) 165.

[41] Y. Liang, S.A. Bradford, J. Šimůnek, E. Klumpp, Mechanisms of graphene oxide aggregation, retention, and release in quartz sand, Sci. Total Environ. 656 (2019) 70–79.

[42] A. Rasmuson, E. Pazmino, S. Assemi, W.P. Johnson, Contribution of nano-to microscale roughness to heterogeneity: closing the gap between unfavorable and favorable colloid attachment conditions, Environ. Sci. Technol. 51 (2017) 2151–2160.

[43] A. Rasmuson, K. VanNess, C.A. Ron, W.P. Johnson, Hydrodynamic versus surface interaction impacts of roughness in closing the gap between favorable and unfavorable colloid transport conditions, Environ. Sci. Technol. 53 (2019) 2450–2459.

[44] S.A. Bradford, S. Torkzaban, Colloid interaction energies for physically and chemically heterogeneous porous media, Langmuir 29 (2013) 3668–3676.

[45] S.A. Bradford, S. Torkzaban, J. Simunek, Modeling colloid transport and retention in saturated porous media under unfavorable attachment conditions, Water Resour. Res. 47 (2011).

[46] T. Tosco, A. Tiraferri, R. Sethi, Ionic strength dependent transport of microparticles in saturated porous media: modeling mobilization and immobilization phenomena under transient chemical conditions, Environ. Sci. Technol. 43 (2009) 4425–4431.

[47] E. Pazmino, J. Trauscht, W.P. Johnson, Release of colloids from primary minimum contact under unfavorable conditions by perturbations in ionic strength and flow rate, Environ. Sci. Technol. 48 (2014) 9227–9235.

[48] W.P. Johnson, E. Pazmino, H. Ma, Direct observations of colloid retention in granular media in the presence of energy barriers, and implications for inferred mechanisms from indirect observations, Water Res. 44 (2010) 1158–1169.

[49] W. Zhang, W. Xia, Z. Lv, Y. Xin, C. Ni, L. Yang, Liquid biopsy for cancer: circulating tumor cells, circulating free DNA or exosomes? Cell. Physiol. Biochem. 41 (2017) 755–768.

[50] Q. Zhang, S.M. Hassanizadeh, B. Liu, J.F. Schijven, N.K. Karadimitriou, Effect of hydrophobicity on colloid transport during two-phase flow in a micromodel, Water Resour. Res. 50 (2014) 7677–7691.

[51] J. Jung, S.C. Cao, Y.-H. Shin, R.I. Al-Raoush, K. Alshibli, J.-W. Choi, A microfluidic pore model to study the migration of fine particles in single-phase and multi-phase flows in porous media, Microsyst. Technol. (2017), https://doi.org/10.1007/s00542-017-3462-1.

[52] S. Nishad, R.I. Al-Raoush, Colloid retention and mobilization mechanisms under different physicochemical conditions in porous media: A micromodel study, Powder Technol. 377 (n.d.) 163–173.

[53] T. Li, Y. Jin, Y. Huang, B. Li, C. Shen, Observed dependence of colloid detachment on the concentration of initially attached colloids and collector surface heterogeneity in porous media, Environ. Sci. Technol. 51 (2017) 2811–2820.

[54] M. Elimelech, C.R. O'Melia, Kinetics of deposition of colloidal particles in porous media, Environ. Sci. Technol. 24 (1990) 1528–1536.

[55] S. Torkzaban, S.A. Bradford, Critical role of surface roughness on colloid retention and release in porous media, Water Res. 88 (2016) 274–284.

[56] S.A. Bradford, S.R. Yates, M. Bettahar, J. Simunek, Physical factors affecting the transport and fate of colloids in saturated porous media, Water Resour. Res. 38 (2002).

[57] D. Zhou, D. Wang, L. Cang, X. Hao, L. Chu, Transport and re-entrainment of soil colloids in saturated packed column: effects of pH and ionic strength, J. Soils Sediments 11 (2011) 491–503.

[58] V. Canseco, A. Djehiche, H. Bertin, A. Omari, Deposition and re-entrainment of model colloids in saturated consolidated porous media: experimental study, Colloids Surfaces A Physicochem. Eng. Asp. 352 (2009) 5–11.